

The rotary subwoofer: A controllable infrasound source

Joseph Park, Milton Garcés^{a)}
University of Hawaii
Infrasound Laboratory
73-4460 Queen Kaahumanu Hwy #119
Kailua-Kona, HI 96740

Bruce Thigpen
Eminent Technologies
225 East Palmer Street
Tallahassee, FL 32301

(Dated: September 30, 2008)

The rotary subwoofer is a novel acoustic transducer capable of projecting infrasonic signals at high sound pressure levels. The projector produces higher acoustic particle velocities than conventional transducers which translate into higher radiated sound pressure levels. This paper characterizes measured performance of a rotary subwoofer and presents a model to predict sound pressure levels.

PACS numbers: 43.20.Rz, 43.28.Dm, 43.28.Hr, 43.38.Ja

I. INTRODUCTION

While considerable technological progress has focused on infrasound sensors, signal processing and propagation effects, fundamental physical barriers have hindered the development of a controllable infrasound source¹. Classic audio transduction technology such as voice-coil activated diaphragms, piezoelectric resonators, and magneto-resistive sheets lack either the large spatial dimensions or vibratory displacements required to effectively radiate high-intensity infrasound.

The literature (as far as is known to the authors) provides no clear demonstration of an efficient, controllable infrasound source; though inventors have explored the limits of conventional loudspeaker technology. For example, the 'hydrosonic subwoofer' used fluid coupling to impedance match infrasound to enclosure vibrations², while optimization of a driven Helmholtz resonator also demonstrated infrasound generation³. However, these devices have peculiar needs such as fluid bladders or require physical changes to tune alternate frequencies. Explosive sources (including air guns) do generate sufficient acoustic pressures, however, they are relatively uncontrollable in amplitude and duration, and are not amenable to continuous-wave sound projection. Such devices also entail a host of environmental and safety issues.

An alternative technology has been recently developed (patent pending) by Eminent Technology^{4,5}, a home & commercial audio speaker manufacturer based in Tallahassee Florida. The projector consists of a baffled fan with dynamically controlled blade pitch and is referred to as the TRW (Thigpen Rotary Woofer). An electric motor rotates the hub at a constant frequency Ω while the blade pitch is dynamically controlled by a signal $s(t)$ at frequency ω_s (figure 1.) In the non-radiating state,

blade pitch is zero with minimal air displacement. In the radiating mode the blade pitch is actively modulated according to the input signal and the resultant pulses of air create high amplitude coherent oscillations in a controlled manner.

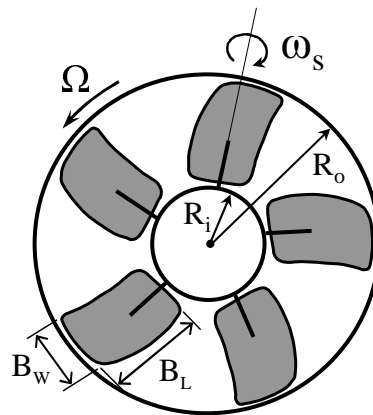


FIG. 1. The rotary subwoofer consists of a hub of radius R_i rotating at a fixed rate of Ω with blades of length B_L and width B_w modulated in pitch by signal $s(t)$ with frequency ω_s .

Classic transduction techniques are limited by poor radiation resistance at small values of ka where k is the wavenumber and a the characteristic dimension of the radiator. For example, a uniformly oscillating piston in a rigid semi-infinite baffle operating at $ka \ll 1$ has a radiation resistance R_r that is close to zero. Efficient radiation doesn't occur until higher frequencies are reached ($ka > 4$) where $R_r \approx 1$. This paper demonstrates that the TRW overcomes this limitation by efficiently projecting relatively high sound pressure levels (SPL) even though the source is compact ($ka \ll 1$). We speculate that the rotary woofer creates an effective R_r ,

^{a)}Electronic address: jpark@isla.hawaii.edu

even though $ka \ll 1$ because it changes the radiation impedance from reactance (mass loading) dominated to resistance (fluid displacement) dominated by virtue of increased particle velocities.

This paper has three main goals: to introduce the rotary subwoofer as a controllable infrasound generator to the acoustics community, to present measurements and performance characterization of the device, and to present a simple theoretical model for the source. The paper is organized as follows: section II provides a physical description of the source and its installation, section III details the measurements and their results. Characterization of the speaker enclosure is explored in this section to explain increased amplitudes of farfield radiation. Section IV presents an acoustic model of the source based on an effective particle velocity distribution. Results of the model are compared with measurements in section V, and discussion of the results are provided.

II. SPEAKER DESCRIPTION AND INSTALLATION

The TRW pitch mechanism uses a conventional electromagnetic voice coil assembly driven by an audio amplifier to pitch the blades in response to the applied signal $s(t)$. The voice coil longitudinal oscillations are converted to blade axis rotary motion within the hub. The tested configuration consisted of 5 equally spaced blades, each approximately $B_w=10.2$ cm (4 in) in width by $B_L=15.3$ cm (6 in) in length. The outer diameter of the hub is approximately 20.4 cm (8 in) so that the annular region of radiation has inner and outer radii of $R_i=10.16$ cm (4 in) and $R_o=25.40$ cm (10 in). The axis of the rotor is approximately 61 cm (24 in) above the ground.

The speaker is installed at the Infrasound Laboratory with the rotor hub and blades flush with a heavy sound board baffle that is clamped inside an exterior door opening with dimensions 91.4 cm (3 ft) x 213.4 cm (7 ft.) The projector radiates into free space outside the building, while the building interior forms the back volume. Figure 2 shows a photograph of the installed source.

The building dimensions are approximately 9.14 m (30 ft) x 18.3 m (60 ft) x 4.3 m (14.2 ft). There are no structural partitions within the building. Construction consists of a bolted steel frame, with W and S-shape I-beams used as columns and beams. Corrugated steel panels are screwed to the frame to form exterior walls and roof. The result is a building with considerable structural compliance compared to a concrete block design. When the rotary woofer is in operation the exterior wall panels are easily observed to oscillate.

III. MEASUREMENTS

Measurements were conducted with calibrated Chapparral Physics Model 2.2A infrasound microphones⁶. Data were recorded and digitized on a RefTek Model 130-01 at a sample frequency of 100 Hz. Input signals were generated by an EZ Digital FG-8002 function generator. The blade actuation signal $s(t)$ was a sine wave

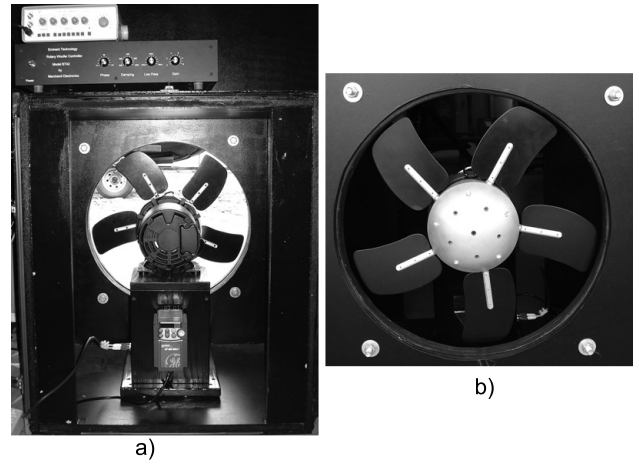


FIG. 2. Photograph of the installed source. a) view inside the building showing the function generator, amplifier, motor controller and motor, b) view from the exterior showing the main rotor hub and blades.

with constant amplitude and frequency ω_s for any given measurement. Minimum record lengths for each measurement were 120 s. Spectral processing used a 50% data overlap with 1024 point Welch's averaged modified periodogram method and a minimum of 25 averages.

Figure 3 plots the spectrum of sound pressure levels for signal frequencies $f_s = \omega_s/2\pi = 2, 4, 8, 16$ Hz recorded on-axis at a range of 1 m with a fan rotational frequency of $F = \Omega/2\pi = 17$ Hz (1020 RPM). Significant harmonic contributions are evident at the lower drive frequencies. It is clear that the source as installed is far from a linear device in the near field at infrasonic frequencies. The primary harmonic generation mechanisms have not yet been identified.

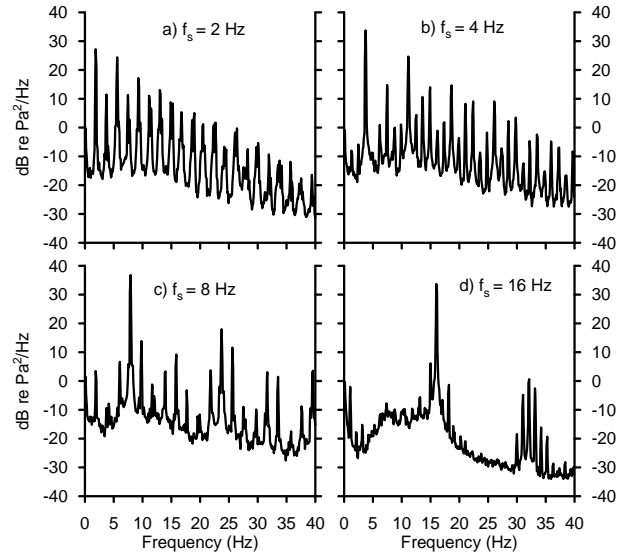


FIG. 3. Acoustic power spectra at a range of 1 m with fan rotation frequency of $F=17$ Hz, and blade pitch modulation frequencies of $f_s=2,4,8,16$ Hz.

Owing to the small atmospheric absorption of infrasound (less than 0.005 dB/km for frequencies below 16Hz)⁷, we were able to easily detect the TRW at considerable distance. Figure 4 shows on-axis spectra recorded at a range of 1820 m for signal frequencies of $f_s = 4, 8, 12, 16$ Hz with a constant fan rotation of $F = 17$ Hz. Figure 4a shows the $f_s = 4$ and 8 Hz results recorded in the morning with light winds and lower noise levels. The $f_s = 4$ Hz signal produced the harmonic at 12 Hz. Figure 4b plots the results at $f_s = 12$ and 16 Hz during a period of higher winds and higher background noise. During the noisier measurement period the 4 Hz signal would not have been detectable without filtering. Even at a range of 1.8 km, there is impressive signal-to-noise ratio exceeding 20 dB for the 12 and 16 Hz projections.

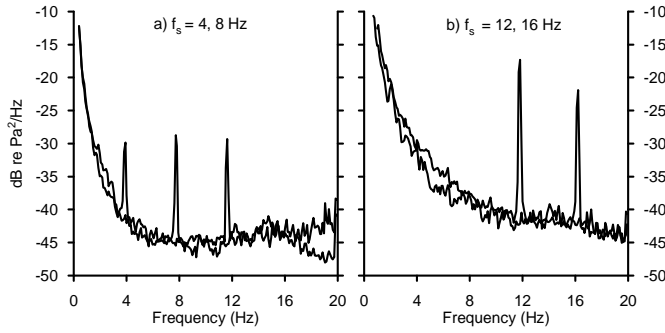


FIG. 4. Acoustic power spectra measured at range of 1820m with fan rotation frequency of $F = 17$ Hz. a) shows signal frequencies of $f_s = 4$ and 8 Hz, b) $f_s = 12$ and 16 Hz.

Figure 5 shows measurements of SPL loss from 1 m for five signal frequencies compared to spherical spreading loss (solid line.) The lack of amplitude fluctuations indicate that there are no nearfield pressure effects, as one would expect for a projector with $kR_o < 0.15$.

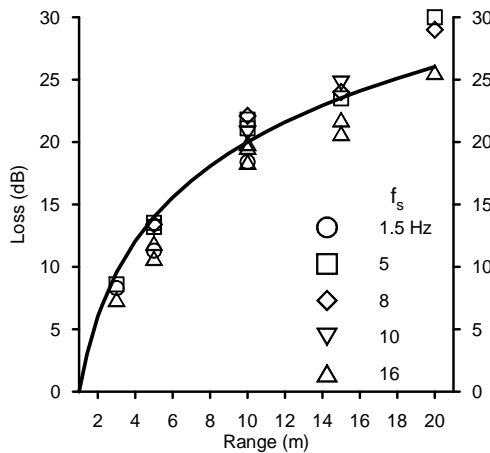


FIG. 5. SPL loss versus range referenced to a distance of 1m at the five signal frequencies $f_s = 1.5, 5, 8, 10, 16$ Hz. The solid curve represents spherical spreading loss.

The acoustic model presented in the following sec-

tion decomposes the particle velocities at the face of the blades into two components. The first is produced by the rotational velocity of the fan about the main hub at frequency F , the other from the rotational velocity of the blade about it's actuation axis at frequency f_s . The component produced from main hub rotation at frequency F will increase in proportion to the frequency F , the radius of the hub, and the outer radius of the blades. The component related to f_s is controlled by the amplitude of the signal $s(t)$, and the rate of blade actuation f_s . As the amplitude of $s(t)$ increases the blade pitch actuation increases driving the blade through larger displacements and higher velocities.

Figures 6 and 7 quantify changes in SPL as a function of the three parameters F , f_s , and $|s(t)|_{RMS}$. To estimate the SPL at a particular signal frequency, a time-series analysis was used. A bandpass filter of 1Hz was centered on the signal frequency, the computed variance provides an estimate of the signal power and is converted into dB.

Figure 6 presents estimates of projector SPL measured at 1 m with a constant $F = 11$ Hz (660 RPM). Values of root mean square (RMS) input signal voltage amplitude ($V_{in} = |s(t)|_{RMS}$) are denoted next to each estimate. It is clear that at this fan rotation frequency the signal frequencies of $f_s = 4, 8$ Hz produce a more efficient response than the lower or higher signal frequencies. It can also be observed that for a specific signal frequency that an increase in signal amplitude (blade pitch actuation) produces an increase in projected SPL.

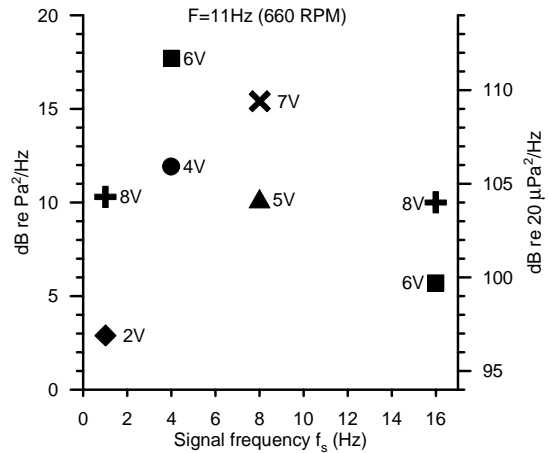


FIG. 6. Estimated source SPL from measurements at 1m with $F = 11$ Hz versus signal frequency f_s . RMS voltage amplitude of the drive signal is denoted next to each measurement.

Estimates of SPL at 1 m with $F = 17$ Hz are shown in figure 7. Compared to the $F = 11$ Hz results, we find significant increases in SPL. Data represented by solid symbols were recorded at a range of 1 m, while the open symbols were recorded at a range of 1820 m and corrected to 1 m based on spherical spreading loss. Peak levels measured at 1 m were 28.1 dB re Pa^2/Hz (122.2 dB re $20\mu\text{Pa}^2/\text{Hz}$).

The estimates at 12 and 16 Hz from the range corrected

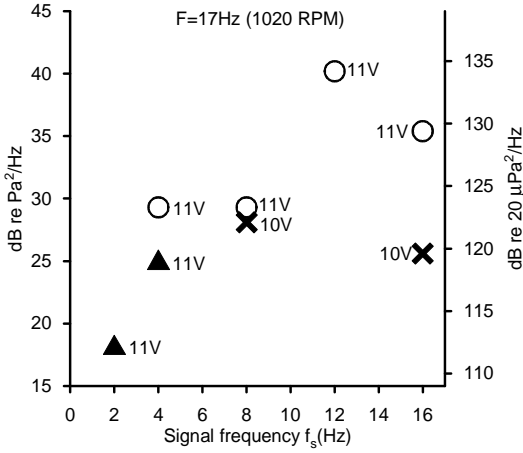


FIG. 7. Estimated source SPL from measurements at 1m and 1820m with $F = 17$ Hz versus signal frequency f_s . RMS voltage amplitude of the drive signal is denoted next to each measurement.

1820 m measurements are unexpectedly high. Two possible mechanisms for this could be changes in the propagation channel, or resonant coupling from the baffle/back volume. It is known that changes in temperature profile and wind conditions can produce a profound impact on the local (<50 km) propagation of infrasound⁸. The measurements at $f_s = 12$ and 16 Hz were performed with a southwest (040°) wind of approximately 4 m/s aligned with the direction with the projector axis (032°), while the $f_s = 4$ and 8 Hz measurements were collected earlier in the day with little or no wind.

Resonant coupling could arise from forced oscillation of the building close to its natural modes. For a rectangular enclosure of dimensions l_x, l_y , lowest axial mode eigenfrequencies in Hz are $\omega_n = c/\pi l_x$ and $\omega_m = c/\pi l_y$, which evaluate to $f_n=9.4$ Hz ($l_x=18.3$ m) and $f_m=18.8$ Hz ($l_y=9.14$ m). When the enclosure is driven at frequency ω , the axial modes can be described by:

$$P_{nm} = \frac{A_{nm} \cos k_n x \cos k_m y}{\sqrt{(1/Q_{nm})^2 + (\omega/\omega_{nm} - \omega_{nm}/\omega)^2}} \quad (1)$$

where A_{nm} is determined by the source and Q_{nm} the quality factor governed by boundary losses⁹. The second term in the denominator describes an amplification (α) factor that maximizes P_{nm} when $\omega = \omega_n$. At a signal frequency of $f_s = 12$ Hz and building eigenfrequency of $f_n = 9.4$ Hz, the value of $\alpha_n = 2.03$. With $f_s = 16$ Hz, $f_m = 18.8$ Hz, $\alpha_m = 3.19$. This suggests that signal frequencies of 12 and 16 Hz are close enough to modal frequencies of the building that there is potential for amplification of building panel oscillation at the drive frequencies. It is therefore possible that the building itself is acting as an extended radiator when driven at signal frequencies of 12 and 16 Hz.

Figure 8 plots a composite transfer function of the output acoustic power at a range of 1 m to the input voltage signal power V_{in} . There are 4 distinct transfer function

spectra plotted in figure 8, a separate measurement at each of the four drive frequencies $f_s = 1, 4, 8$ and 16 Hz, with a constant fan rotation frequency of $F = 11$ Hz. Portions of each spectra were plotted only if the input/output coherence was greater than 0.98. Interpreting the coherence as a metric of input/output linearity, we can see that as the drive frequency increases the spectral band over which the assumed linear response is valid increases, though in none of the measurements does it cover the entire spectrum. A possible reason is that as the drive frequency decreases the increasing compliance of the diaphragm may decouple the input/output.

Turning attention to the amplitude of the transfer functions, the TRW exhibits maximal power conversion over the 3 to 8 Hz band at this F . This is consistent with the measurements presented in figure 6. A notable result of figure 8 are the relatively large amplitudes (> -4 dB), which indicate a high transduction efficiency despite the low value of kR_o .

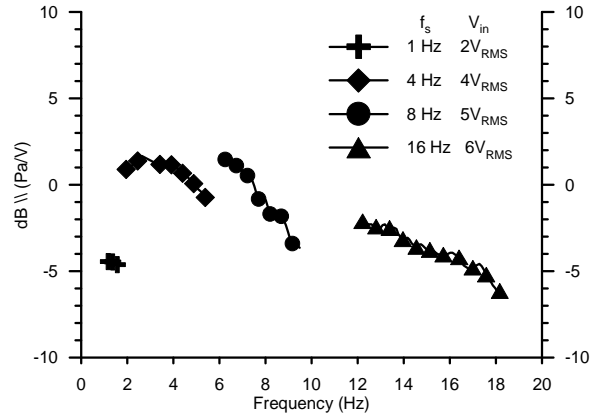


FIG. 8. Composite signal transfer function with values of coherence >0.98 .

A five-point angular response of the projector at a range of 1 m is shown in figure 9. At the low wavenumbers and small radiator dimensions ($kR_o < 0.15$) of the TRW, the radiation field of a baffled simple source should be monopole. The data show a persistent reduction of approximately 2 dB on-axis for all measurements, with similar results at a range of 10 m. Reasons for this departure from the expected omnidirectional radiation are not clear. Evaluation with the source model discussed below indicate that radiation from the wall/baffle is capable of reducing the on-axis pressure.

IV. ACOUSTIC MODEL

The TRW relies on the rotary motion of the hub and blades to generate significant particle velocities, while the dynamically controlled blade pitch creates the fluctuating signal pressure pulses. These two components are similar to those found in cooling/turbo-machinery fans and helicopter rotor blades, both of which have been extensively studied. There are however some differences.

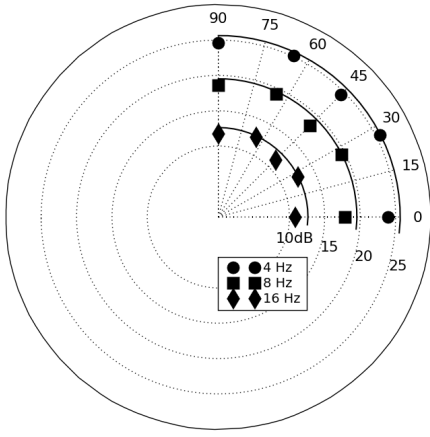


FIG. 9. Angular response measured at a range of 1m for the drive frequencies $f_s=4, 8, 16$ Hz. Data are SPL in units of Pa^2/Hz . The axis of the fan is aligned at 0° .

Fan studies are typically assessed with inclusion of duct or strut interactions, the authors are not aware of cases where the blade pitch is dynamically modulated to produce a desired output signal. Fans have been shown to generate discrete tones as the blades encounter ingested turbulence leading to uneven pressure distributions across the blade^{10–13}, which is analogous to the controlled fluctuations of the TRW. Helicopter rotors conspicuously generate discrete sound from turbulence or vortex interactions^{11,14}, though the main rotors are not baffled and the blade pitch is not modulated at a signal frequency.

An in-depth analysis of the TRW radiation might employ the Ffowcs Williams-Hawkings extension of Lighthill’s acoustic analogy applied to sources in motion^{14,15}, or, evaluation of Kirchoff’s integral for moving surfaces^{16,17}. In the case that the blades can be considered point sources in the low-frequency limit, the method of Morfey could be applied¹⁸. All of these methods require significant resource investments for successful application. Instead, we will use Rayleigh’s integral based on an effective particle velocity to estimate pressure distributions of the projector.

Considering the baffled fan as a planar radiator producing an effective annular surface normal velocity $U_n(S)$, a Green’s function form of the Rayleigh integral may be used to represent the pressure at the field point \mathbf{x} .

$$p(\mathbf{x}) = \frac{i\omega\rho}{2\pi} \int U_n(S) \frac{e^{jk_r r}}{r} dS \quad (2)$$

where ρ is the atmospheric density and r the magnitude of the position vector from the center of the fan to the field point.

With the fan rotational frequency Ω greater than the blade modulation frequency ω_s , we assume that the net

result of forcing on the surrounding air is production of coherent annular rings of pressure pulses. The effective particle velocity of the ring is modeled by assuming superposition of the blade rotational velocity, U_Ω , with the particle velocity U_ω induced by the dynamically adjusted blade pitch.

Figure 10 depicts velocity distributions of the blade along the transverse and longitudinal directions. The velocity along the length of the blade (dimension B_L in figures 1 and 10) is $U_\Omega(R) = \Omega(R_i + R)$, where R is the radial distance from the hub center and takes values in the range $[R_i, R_o]$. An effective velocity evaluated at the centroid of the distribution gives: $\bar{U}_\Omega = \Omega[R_i + 2(R_o - R_i)/3]$. Across the width of the blade (dimension B_W) the velocity is ωR_w , with $R_w \in [0, \pm B_W/2]$, and an effective value can be specified as $\bar{U}_\omega = \pm\omega 2B_W/3$.

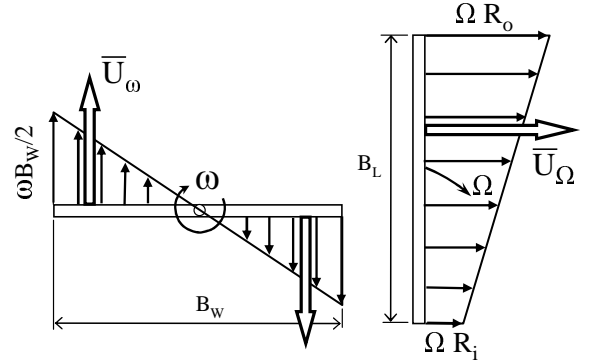


FIG. 10. Blade velocity distributions from the blade pitch modulation frequency ω and the fan rotation Ω .

As the blade varies its angle of attack (θ) according to the signal $s(t)$, the normal component of U_Ω will vary as $\hat{n}\bar{U}_\Omega = \sin(\theta)\bar{U}_\Omega$, as shown in figure 11. The composite particle velocity normal to the blade is then

$$\bar{U}_n = \bar{U}_\omega + \hat{n}\bar{U}_\Omega. \quad (3)$$

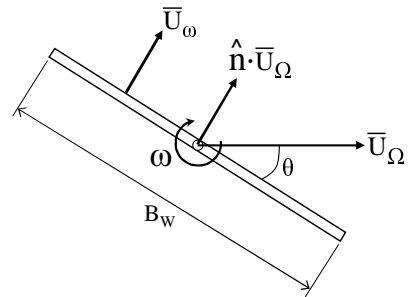


FIG. 11. Effective particle velocity normal to the blade is modeled as the sum of the normal component of fan rotational velocity $\hat{n}\bar{U}_\Omega$ with the effective velocity from the blade pitch modulation \bar{U}_ω .

The maximal value of $\hat{n}\bar{U}_\Omega$ will correspond to the largest excursion of blade pitch $\theta = \theta_{max}$ during ap-

TABLE I. Blade pitch angles θ_{max} in degrees as a function of RMS input signal voltage V_{in} .

V_{in}	2	3	4	5	6	7	8	9	10	11
θ_{max}	25.0	28.8	32.5	36.3	40.0	43.8	47.5	51.3	55.0	58.8

plication of the signal $s(t)$. Since we are interested in pressure amplitude we will evaluate $\hat{n}\bar{U}_\Omega$ at θ_{max} with the assumption that the maximal particle velocity is the primary contributor to the pressure maxima.

Equation 3 is used in equation 2 to compute the radiated pressure of the fan. Equation 2 is numerically evaluated over a grid covering the annular area between the fan hub and baffle. The grid consists of 732 elements of area 2.32 cm^2 each.

The only variable of the model that is not precisely determined is θ_{max} . This value is directly dependent on the amplitude of the input signal V_{in} . While we were able to measure V_{in} , we did not have access to instrumentation that could quantify θ under operating conditions. Observation of the blades indicated that typical values of θ_{max} varied between $25\text{-}60^\circ$ with V_{in} in the range of 2-11 V_{RMS} . Based on this observation we assume a linear relation between V_{in} and θ_{max} with values listed in table I.

V. RESULTS AND DISCUSSION

A. Model Results

Results of equation 2 compared to measured data at a fan rotational frequency of $F = 17 \text{ Hz}$ are shown in table II. Model results are within 2 dB of measured data at drive frequencies of $f_s = 2, 4$ and 8 Hz . However at 16 Hz the pressure is overestimated by 11 dB. The measured data follow the trend of the transfer function such that the output at $f_s = 16 \text{ Hz}$ is about 3 dB down from the output at $f_s = 8 \text{ Hz}$, while the model predicts a 6 dB increase. This could indicate that the blade actuation component of the particle velocity \bar{U}_ω is higher in the model than in the physical system, or that the linear combination of the blade rotation and actuation velocities is no longer a valid representation of the particle velocities.

TABLE II. Model results for a fan speed of 17 Hz (1020 RPM) compared to measured values (SPL) at a range of 1 m. Data and model SPL are dB *re* Pa^2/Hz .

f_s (Hz)	V_{in}	θ_{max}	Ω/ω_s	$\bar{U}_\Omega/\bar{U}_\omega$	SPL	Model
2	11	58.8°	8.5	57.5	18.3	17.7
4	11	58.8°	4.3	28.7	25.1	23.8
8	10	55.0°	2.1	13.7	28.1	29.8
16	10	55.0°	1.1	6.9	25.6	36.4

Examination of the ratio of fan rotation frequency to blade actuation frequency, Ω/ω_s , and of $\bar{U}_\Omega/\bar{U}_\omega$, re-

veals that the model breaks down when $\Omega/\omega_s < 2$ or $\bar{U}_\Omega/\bar{U}_\omega < 10$. This indicates that our assumption for model validity, that the fan rotational frequency Ω should be greater than the blade modulation frequency ω_s to produce coherent pressure pulses that can be modeled with an effective velocity distribution was off by a factor of 2.

Model results compared to measured data with $F = 11 \text{ Hz}$ are presented in table III. At signal frequencies of $f_s = 1$ and 4 Hz the predicted and measured values are within 5 dB, however at the higher frequencies the pressures are severely overpredicted. These results follow the conditions observed above where the model breaks down for $\Omega/\omega_s < 2$ or $\bar{U}_\Omega/\bar{U}_\omega < 10$.

TABLE III. Model results for a fan speed of 11 Hz (660 RPM) compared to measured values (SPL) at a range of 1 m. Data and model SPL are dB *re* Pa^2/Hz .

f_s (Hz)	V_{in}	θ_{max}	Ω/ω	$\bar{V}_\Omega/\bar{V}_\omega$	SPL	Model
1	2	25.0°	11	37.2	2.9	1.9
1	8	47.5°	11	65.4	10.3	6.7
4	4	32.5°	2.8	12.0	11.9	16.6
4	6	40.0°	2.8	14.1	17.7	18.0
8	5	36.3°	1.4	6.6	10.2	23.9
8	7	43.8°	1.4	7.6	15.4	25.1
16	6	40.0°	0.7	3.6	5.7	31.6
16	8	47.5°	0.7	4.1	10.0	32.4

B. Discussion

We have decomposed the effective particle velocity of the TRW into two components, the blade rotational velocity, U_Ω , and the signal modulated blade pitch velocity U_ω . Comparison of the magnitude of these components reveals that the electric motor that drives the hub and blades at frequency Ω is the primary accelerator of the particle velocity. For example, at $F = 17 \text{ Hz}$ and $f_s = 8 \text{ Hz}$ the normal component of effective particle velocity from the hub rotation is $\bar{U}_\Omega = 12.3 \text{ m/s}$ while the blade actuation velocity is $\bar{U}_\omega = 1.3 \text{ m/s}$. The majority of the consumed power is used to drive the motor and rotate the hub, on the order of 100 Watts, while the power consumed by the signal actuating the blades is roughly 10 Watts. This relatively small value of signal power producing high levels of acoustic power result in large transfer function amplitudes and good transduction efficiency.

Measurements of radiated sound power found SPL levels at a range of 1 m of 28 dB *re* Pa^2/Hz (122 dB *re* $20\mu\text{Pa}^2/\text{Hz}$). It was clearly demonstrated that increasing the value of rotor velocity, or blade pitch actuation produced increases in SPL. This is consistent with the expectation that increased particle velocities are a contributing factor to TRW performance. Measured values of SPL at a range of 1820 m found significant signal-to-noise ratio's, indicating that detection ranges of the TRW infrasound could exceed 2 km. Unexpectedly high values of SPL were recorded at 12 and 16 Hz at a range of

1820m. It is suggested that the building which forms the back volume of the TRW is resonating at these drive frequencies, which may increase the farfield SPL. Another candidate mechanism for the increased levels are changes in atmospheric propagation conditions. Further study is warranted to research this discrepancy.

A coarse measurement of angular response found reasonable agreement with monopole radiation as expected for a baffled source with $kR_o \ll 1$. However, a roughly 2 dB reduction in the on-axis response was observed at all frequencies. Use of the Rayleigh integral model indicates that radiation from the building wall may be contributing to this, though reduction in SPL of 2 dB could not be reproduced. This represents another area where additional research is needed.

A simple model based on effective particle velocities applied to Rayleigh's integral was developed to predict radiated pressures. The model assumes that the velocity distribution can be considered a linear superposition of effective blade velocities from the fan rotation and the blade pitch actuation. Model results at $F = 17$ Hz were within 2 dB of measured values at signal frequencies of $f_s = 2, 4, 8$ Hz, but overpredicted pressure by 11 dB at $f_s = 16$ Hz. Model values at $F = 11$ Hz were within 5 dB at $f_s = 1$ and 4 Hz, but were too large by more than 10 dB for $f_s = 8$ and 16 Hz. It was observed that when $\Omega/\omega_s < 2$ the model results are poor. This may be an indication that the effective particle velocity representation is no longer valid. A detailed model with improved particle velocity distributions and analysis methods are suggested to address this problem.

VI. CONCLUSION

The rotary subwoofer is a novel acoustic transducer capable of efficiently generating controllable infrasound signals at high sound pressure levels. It is suggested that the TRW overcomes the canonical difficulty of conventional transducers operating in the infrasound band, that the radiation resistance is near zero since the radiation impedance is dominated by mass-loading, by changing the impedance to fluid displacement dominated by virtue of increased particle velocities. Another unique aspect of the rotary subwoofer is the high transduction efficiency in terms of input signal power to radiated sound power.

The development of a controllable infrasound generator will likely find utility in several acoustic applications. For example, the field calibration of infrasound arrays operated by the International Monitoring System (IMS) of the Comprehensive Test Ban Treaty Organization (CTBTO), and as a tool for assessing atmospheric propagation studies. Other applications might include the field simulation of geophysical or anthropogenic infrasound sources to assist in the development of infrasound sensors and detection algorithms.

Acknowledgments

We wish to acknowledge the support of the National Consortium for Measures and Signatures Intelligence (MASINT) Research (NCMR).

- ¹ Bedard, B. J. and Georges, T. M., "Atmospheric Infrasound", *Physics Today*, March 2000, 32-37 (2000).
- ² Alton Jr., Noyal J., Fluid damped acoustic enclosure system, United States Patent 5,281,777, Filed March 2, 1993, granted January 25, 1994.
- ³ Domen, John K., Infrasonic Helmholtz resonator, United States Patent 6,665,413, Filed July 22, 2002, granted December 16, 2003.
- ⁴ Eminent Technologies, 225 East Palmer Street, Tallahassee, FL 32301, <http://www.eminent-tech.com/main.html>, accessed June 12, 2008.
- ⁵ Garcés M. and , Park, J., "A rotary subwoofer as an infrasonic source", 2007 Infrasonic Technology Workshop, November 13-16, 2007, Tokyo, Japan.
- ⁶ Chaparral Physics, Geophysical Institute, University of Alaska, P.O. Box 757320, Fairbanks, AK 99775-7320, <http://www.gi.alaska.edu/chaparral/>, accessed June 12, 2008.
- ⁷ Sutherland, L. C. and Bass, H. E., "Atmospheric absorption at high altitudes", *J. Acoust. Soc. Am.*, **115**(3), 1012-32, (2004).
- ⁸ Fee, David and Garcés, Milton "Infrasonic tremor in the diffraction zone", *Geophys. Res. Lett.*, **34**, doi:10.1029/2007GL030616, L16826 (2007).
- ⁹ Kinsler, Lawrence E., *Fundamentals of Acoustics*, 3rd Ed., 334, John Wiley & Sons, ISBN 0-471-02933-5, (1982).
- ¹⁰ Mani, R., "Noise due to interaction of inlet turbulence with isolated stators and rotors", *J. Sound Vib.*, **17**(2), 251-60 (1971).
- ¹¹ Wright, S. E., "Discrete radiation from rotating periodic sources", *J. Sound Vib.*, **17**(4), 437-98 (1971).
- ¹² Chiu Wen-Shyang, Lauchle G. C., Thompson, D. E., "Subsonic axial flow fan noise and unsteady rotor force", *J. Acoust. Soc. Am.*, **85**(2), 641-7 (1989).
- ¹³ Majumdar and S. J., Peake, N., "Noise generation by the interaction between ingested turbulence and a rotating fan", *J. Fluid Mech.*, **359**, 181-216 (1998).
- ¹⁴ Brentner and K. S., Farassat, F., "Modeling aerodynamically generated sound of helicopter rotors", *Prog. Aerospace Sci.*, **39**(2), 83-102 (2003).
- ¹⁵ Ffowcs Williams, J. E. and Hawkings, D. L., "Sound generation by turbulence and surfaces in arbitrary motion", *Phil. T. R. Soc. London Ser. A*, **264**, 321-42 (1969).
- ¹⁶ Farassat, F. and Myers, M. K., "Extension of Kirchoff's formula to radiation from moving surfaces", *J. Sound Vib.*, **123**(3), 451-9 (1988).
- ¹⁷ Myers, M. K. and Hausmann, J. S., "On the application of the Kirchoff formula for moving surfaces", *J. Sound Vib.*, **139**(1), 174-8 (1990).
- ¹⁸ Morfey, C. L. and Tanna, H. K., "Sound radiation from a point force in circular motion", *J. Sound Vib.*, **15** 325-351 (1971).